Analysis of TCC in p-n short silicon diodes at 300–400 K

R. Kubica, A. Albouy, F. Balestra, A. Aliane, P. Leduc

Analysis of TCC in p-n Short Silicon Diodes at 300–400 K

R. M. R. Kubica, A. Albouy, F. Balestra, *Senior Member, IEEE*, A. Aliane, and P. Leduc

***Abstract* — This work presents a study of the thermal sensitivity of p-n short silicon diodes represented by the temperature coefficient of current (TCC) for thermal sensing applications. It proposes an analytical model (AM) of the TCC of p-n short silicon diodes under low-level injections and in the temperature range of 300–400 K. First, the TCC is studied at diffusion and recombination regimes and it is discriminated between different physical contributions. Then, it is followed by a discussion on the origins and influences of these contributions to provide a usable and simplified analytical expression of the TCC. Finally, the proposed AM is compared to technology computer-aided design (TCAD) simulations and experimental results at 300–400 K. It shows a strong correlation for different designs of p-n short diodes.**

***Index Terms*— Analytical model (AM), p-n-diode, short diode, silicon, technology computer-aided design (TCAD), temperature coefficient of current (TCC), thermal sensitivity, thermal sensors.**

I. Introduction

THERMAL sensors are widely used in various fields of application. This includes, for example, electrotechnical and automotive systems, industrial control, medical devices, smartphones, and other defense or security systems. All of these electronic sensors are based on various technologies [1], [2] such as thermocouples [3], thermistors [4], [5], or diode temperature sensors [6]. The performances of these sensors are driven by three main factors: sensitivity, noise, and operational temperature. Sensitivity is assessed using the temperature coefficient of X (TCX) (% · K^{-1}) [1], [2], [7]

$$\mathrm{TCX} = \frac{1}{X}\frac{dX}{dT} \tag{1}$$

where T is the temperature (K) and X is a parameter sensitive to T (resistance, current, and voltage) which depends on the technology of the sensor.

Thermistors are characterized by their temperature coefficient of resistance (TCR) with typical values from −1% K^{-1} to −3% K^{-1} [5]. Whereas, diode thermometers are characterized by the temperature coefficient of voltage (TCV) [6], [8] or the temperature coefficient of current (TCC) [9], [11], [12]. In general, TCC of silicon p-n diodes is higher than TCR of thermistor materials, but depends on the applied voltage. Moreover, silicon diodes are compatible with foundry manufacturing processes and their production costs are low. They are, therefore, well-suited for thermal sensors. The TCC needs consequently to be physically understood and modeled, especially for low-level minority injections where the TCC is high. Previous works on silicon p-n diodes have already been done to express the TCC in forward bias at 300 K. These studies were either performed on long diodes or on diodes where the current density was only dominated by the diffusion of minority carriers [9], [10], [11], [12], [13]. The present article proposes to extend the study to forward-biased short diodes between 300 and 400 K. This work aims to establish a model sufficiently simple to lead a physical general analysis of the TCC and not to propose a complete compact model. The model includes parameters such as the doping concentration, carrier lifetime, and diode length. The impact of these parameters on the TCC is assessed to provide a simplified expression. Finally, our model of TCC is compared to technology computer-aided design (TCAD) simulations and experimental results at 300–400 K.

II. AM of the TCC in p-n Diodes

The p-n diode is one of the most basic structures in microelectronics. Made by the juxtaposition of two semiconductors (P and N), the current–voltage characteristic of a p-n diode is nonlinear. Under forward bias, the current density J (A m^{-2}) of the diode depends on three mechanisms [14]: diffusion of minority charge carriers, recombination of minority charge carriers, and the drift of charge carriers due to the series resistance R_s (▲). J_{diff} and J_{rec} represent the current density due to the diffusion and the recombination of minority charge carriers (A·m^{-2}). To express these currents, we used the following hypotheses and notations.

1) The p-n junction is made of silicon, is considered abrupt at thermal equilibrium, and is studied at 300–400 K.

Manuscript received 14 March 2024; revised 18 April 2024 and 23 May 2024; accepted 29 May 2024. Date of publication 11 June 2024; date of current version 25 July 2024. This work was supported in part by Directorate General of Armament (DGA) from the French Ministry of Defense, in part by Important Project of Common European Interest (IPCEI) Microelectronics and Connectivity, and in part by the French Public Authorities within the frame of France 2030. The review of this article was arranged by Editor K. Xia. *(Corresponding author: R. M. R. Kubica.)*

R. M. R. Kubica, A. Albouy, A. Aliane, and P. Leduc are with the Grenoble-Alpes University, 38400 Grenoble, France, and also with CEA Leti, 38054 Grenoble, France (e-mail: romain.kubica@cea.fr; antoine.albouy@cea.fr; abdelkader.aliane@cea.fr; patrick.leduc@cea.fr).

F. Balestra is with CNRS, Grenoble-INP, CROMA, Grenoble-Alpes University, 38000 Grenoble, France (e-mail: francis.balestra@grenoble-inp.fr).

Color versions of one or more figures in this article are available at https://doi.org/10.1109/TED.2024.3408772.

Digital Object Identifier 10.1109/TED.2024.3408772

2) Fermi statistics is reduced to Boltzmann statistics to describe electron distributions on energy levels.
3) The lengths of the P and N regions are l_p and l_n (nm).
4) The doping concentrations in the P and N regions are N_a and N_d (at $\cdot$ cm^{-3}).
5) Due to the bandgap narrowing effect, the concentrations of intrinsic carriers n_i are different in the P and N regions and noted n_{ip} and n_{in} (at $\cdot$cm^{-3}).
6) The lengths of the space charge regions in the P and N regions are W_p and W_n (nm).
7) The diffusion coefficients of minority charge carriers (m^2 $\cdot$ s^{-1}) in the P and N regions are D_p and D_n.
8) The lifetimes of the charge carriers in the P and N regions are τ_p and τ_n (s).
9) The diode is supposed short, that is, $l_{p,n}$ are small compared to the diffusion lengths of the charge carriers.
10) The recombination mechanisms are only provided by SRH-type mechanisms [16], [17].
11) The behavior of the diode is studied at low-level minority carriers injections. Therefore, the influences of R_s and the self-heating are neglected.

The following expressions are used for J [14]:

$$J = J_{\text{diff}} + J_{\text{rec}}. \tag{2}$$

With

$$J_{\text{diff}} = J_{\text{diff-sat}} \left(\exp\left(\frac{qV_a}{kT}\right) - 1 \right) \tag{3}$$

$$J_{\text{rec}} = q \int_0^W U(x)\,dx \tag{4}$$

where V_a is the applied voltage to the diode (V) and $J_{\text{diff-sat}}$ represents the saturation current density linked to diffusion (A $\cdot$ m^{-2}) [14]

$$J_{\text{diff-sat}} = q \left(\frac{D_n n_{\text{in}}^2}{(l_n - W_n)N_d} + \frac{D_p n_{\text{ip}}^2}{(l_p - W_p)N_a} \right). \tag{5}$$

In (4), W is the total length of the space charge region (m) and U is the recombination rate (m^{-3} $\cdot$ s^{-1}) [14]

$$U = \frac{np - n_i^2}{\tau_h \left[n + n_i \exp\left(\frac{E_t - E_i}{kT}\right) \right] + \tau_e \left[p + n_i \exp\left(\frac{E_i - E_t}{kT}\right) \right]} \tag{6}$$

where n and p are the electron and hole concentrations (at $\cdot$ cm^{-3}), $\tau_{e,h}$ are the lifetime of electrons and holes (s), E_i is the energy level of the midgap (eV), and E_t is the energy level associated with the recombination mechanisms (eV).

Then, we assume the following hypotheses to simplify (6).
1) The lifetimes of electrons and holes are equal ($\tau_{e,h} = \tau$).
2) The np product is constant in W.
3) The recombination occurs at the midgap ($E_t = E_i$).

Therefore, U is equal to

$$U = \frac{n_i^2 \left(\exp\left(\frac{qV_a}{kT}\right) - 1 \right)}{\tau(n + p + 2n_i)}. \tag{7}$$

U varies in W because the sum $n + p$ depends on the minimal [14]. The maximum recombination rate $U_{\max}$ is noted

$$U_{\max} = \frac{n_i \left(\exp\left(\frac{qV_a}{kT}\right) - 1 \right)}{2\tau \left(\exp\left(\frac{qV_a}{2kT}\right) + 1 \right)} \simeq \frac{n_i \left(\exp\left(\frac{qV_a}{2kT}\right) - 1 \right)}{2\tau}. \tag{8}$$

To provide an usable expression for J_{rec}, (8) is usually considered to be valid in W ($U = U_{\max}$). However, this approximation overestimates the value of J_{rec}. Therefore, we choose to use expressions proposed by Shur [18] where J_{rec} is expressed

$$J_{\text{rec}} \simeq q \cdot \sqrt{\frac{2\pi (U_{\max})^3}{|U_0''|}} \tag{9}$$

where U_0'' is the second derivative of the recombination rate U near x_0 where $n = p$. Then, (9) is approximated to obtain

$$J_{\text{rec}} = J_{\text{rec-sat}} \exp\left(\frac{qV_a}{2kT}\right). \tag{10}$$

With $J_{\text{rec-sat}}$ represents the saturation current density linked to the recombination (A $\cdot$ m^{-2}) [18]

$$J_{\text{rec-sat}} = \frac{\pi}{2} \sqrt{\frac{kT}{F_{np}^2}} n_i \tau^{-1} \tag{11}$$

where F_{np} is the electric field at the junction between the P and N regions (V $\cdot$ m^{-1}).

Given these expressions of J, the TCC can be expressed when $J = J_{\text{diff}}$ (TCC_{diff}) and $J = J_{\text{rec}}$ (TCC_{rec}) [9], [13].

A. Temperature Coefficient of Diffusion Current

In the case of $J = J_{\text{diff}}$, the TCC is expressed as follows:

$$\text{TCC}_{\text{diff}} = \frac{1}{J_{\text{diff}}} \frac{dJ_{\text{diff}}}{dT}. \tag{12}$$

Assuming that $\exp(qV_a)/(kT) \gg 1$ and by using (3), the following expression of the TCC_{diff} is obtained:

$$\text{TCC}_{\text{diff}} = \frac{1}{J_{\text{diff-sat}}} \frac{dJ_{\text{diff-sat}}}{dT} - \frac{qV_a}{kT^2}. \tag{13}$$

Nevertheless, for a better understanding of the TCC_{diff}, (13) is discriminated into different physical parameters. Thus, $J_{\text{diff-sat}}$ is developed, and the contributions of the N and P regions ($J_{\text{diff-sat}n}$ and $J_{\text{diff-sat}p}$) are separated

$$J_{\text{diff-sat}} = J_{\text{diff-sat}n} + J_{\text{diff-sat}p}. \tag{14}$$

With

$$J_{\text{diff-sat}n,p} = q_p \frac{D_{n,p} n_{\text{in},p}^2}{(l - W_{n,p})N_{d,a}}. \tag{15}$$

Then, (15) is developed by separating the contributions of $J_{\text{diff-sat}n,p}$ using the logarithmic derivative and (1)

$$\frac{dJ_{\text{diff-sat}n,p}}{J_{\text{diff-sat}n,p}} = \text{TCD}_{n,p} + \text{TCNI}_{n2,p2} - \text{TCLW}_{n,p} \tag{16}$$

location. It reaches a maximum when the sum $n + p$ is $J_{\text{diff}-\text{sat}n,\,p} \cdot dT$

where $TCD_{n,p}$, $TCNI_{n2,p2}$ and $TCLW_{n,p}$ are the temperature coefficients of $D_{n,p}$, $n^2_{in,p}$ and $l - W_{n,p}$. This expression of the TCC_{diff} is thus obtained

$$TCC_{diff} = \frac{J_{diff-satn}}{J_{diff-sat}}(TCD_n + TCNI_{n2} - TCLW_n) + \frac{J_{diff-sat\ p}}{J_{diff-sat}}(TCD_p + TCNI_{p2} - TCLW_p) - \frac{qV_a}{kT^2}. \quad (17)$$

If p^+n or n^+p diodes are considered, $J_{diff-sat}$ depends only on one region (P or N). For a n^+p diode ($J_{diff-sat} \approx J_{diff-sat\ p}$), (17) is approximated

$$TCC_{diff} \approx TCD_p + TCNI_{p2} - TCLW_p - \frac{qV_a}{kT^2}. \quad (18)$$

1) Temperature Coefficient of Diffusion Coefficients: Considering a nondegenerated semiconductor, $D_{n,p}$ can be written using the Einstein relation [14]

$$D_{n\ p} = \mu_{n\ p}\frac{kT}{q} \quad (19)$$

where $\mu_{n,p}$ are the mobilities of charge carriers ($m^2 \cdot V^{-1} \cdot s^{-1}$). Assuming that the electric field E is low enough, the mobility saturation effects are neglected. The minority charge carriers are in equilibrium with the lattice and $\mu_{n,p}$ are dependent on phonons and impurities concentrations N_T ($at \cdot cm^{-3}$). Moreover, E is considered to be applied in the same direction as the charge carriers' movement. Under these conditions, the expression of $\mu_{n,p}$ is obtained [14], [20]

$$\mu_{n,p} = \mu_{n,p-300\,K}\left(\frac{300}{T}\right)^{\delta} \quad (20)$$

where $\mu_{n,p-300\,K}$ represent the mobilities of minority charge carriers at 300 K and δ is a parameter between 1.5 and 2.7 [20], [21], [22]. We choose to fix δ such as $\delta = 1.5$. We calculated $\mu_{n,p-300\,K}$ using the Masetti et al. [23] model. By using (19) and (20), (21) is obtained to express $D_{n,p}$

$$D_{n,p} = C_{Dn,p} \cdot T^{1-\delta}. \quad (21)$$

The parameter $C_{Dn,p} = (k/q)\mu_{n,p-300\,K}300^{\delta}$ is independent of T. Therefore, the $TCD_{n,p}$ is expressed as

$$TCD = TCD_{n\ p} = \frac{1}{D_{n,p}}\frac{dD_{n,p}}{dT} = (1-\delta)\cdot T^{-\delta}. \quad (22)$$

2) Temperature Coefficient of the Square of the Concentration of Intrinsic Carriers: These forms are used for $n_{in,p}$ [15]

$$n_{in,p} = \sqrt{N_c N_v}\left(\frac{T}{300}\right)^{\frac{3}{2}}\exp\left(-\frac{qE_{gn,p}}{2kT}\right) \quad (23)$$

where $N_{c,v}$ are the effective density of states for the conduction and the valence bands at 300 K (m^{-3}) and $E_{gn,p}$ are the bandgaps in N and P regions (eV).

We consider that $E_{gn,p}$ is dependent on T according to *Varshni's* empirical equation [14], [24], [25]. On the other hand, the *Slotboom*'s law is used for the bandgap narrowing [26]

$$E_{gn,p} = E_{gn0,p0} - \frac{\alpha T^2}{T+\beta}. \quad (24)$$

With

$$E_{gn0,p0} = 1,17 - \gamma_1\ln\left(\frac{N_T}{\gamma_2}\right) + \sqrt{\ln\left(\frac{N_T}{\gamma_2}\right)^2 + \gamma_3} \quad (25)$$

where $E_{gn0,p0}$ are the bandgaps in N and P regions (in eV) at 0 K and α, β, γ_1, γ_2, and γ_3 are constants. In this article, we consider that $N_T = N_{d,a}$ for N and P regions.

Finally, by using (24) and (25), we express $TCNI_{n2,p2}$

$$TCNI_{n2,p2} = \frac{1}{n^2_{in,p}}\frac{dn^2_{in,p}}{dT} = \frac{3}{T} + \frac{q}{k}\frac{E_{gn0,p0}}{T^2} + \frac{\alpha\beta}{(T+\beta)^2}. \quad (26)$$

3) Temperature Coefficient of the Lengths of Neutral Regions: The expression of $TCLW_{n,p}$ is simplified as

$$TCLW_{n,p} = \frac{d(l_{n,p} - W_{n,p})}{(l_{n,p} - W_{n,p})dT} = \frac{1}{W_{n,p} - l_{n,p}}\frac{dW_{n,p}}{dT}. \quad (27)$$

Then, the expressions of $W_{n,p}$ are developed [14]

$$W_{n,p} = C_{wn,p}\sqrt{\Phi_0 - V_a}. \quad (28)$$

With

$$C_{wn} = \sqrt{\frac{2\epsilon_0\epsilon_r}{q(N_d+N_a)}\frac{N_a}{N_d}}, \quad C_{wp} = \sqrt{\frac{2\epsilon_0\epsilon_r}{q(N_d+N_a)}\frac{N_d}{N_a}} \quad (29)$$

$$\Phi_0 = \frac{kT}{q}\ln\left(\frac{N_d N_a}{n_{in}n_{ip}}\right) \quad (30)$$

where Φ_0 is the diffusion voltage (V) and $C_{wn,p}$ are parameters independent of T.

Then, the derivative of (28) with respect to T is calculated to obtain

$$\frac{dW_{n,p}}{dT} = \frac{C_{wn,p}}{2\sqrt{\Phi_0 - V_a}}\frac{d\Phi_0}{dT}. \quad (31)$$

By using (28) and (31), $TCLW_{n,p}$ is expressed as

$$TCLW_{n,p} = \frac{-C_{wn,p}\sqrt{\Phi_0 - V_a}}{2(l_{n,p} - C_{wn,p}\sqrt{\Phi_0 - V_a})\sqrt{\Phi_0 - V_a}} \times \frac{d\Phi_0}{dT}. \quad (32)$$

4) Analysis of the Contributions to the Temperature Coefficient of Diffusion Current: Fig. 1 illustrates the results of the TCC_{diff} of a n^+p diode (D1). The TCC_{diff} and its parameters are represented as a function of V_a using (18) at 300 K. In Fig. 1, the TCC_{diff} decreases when V_a increases. In this example, its value goes from 14.5% $\cdot K^{-1}$ to 4.05% $\cdot K^{-1}$ for V_a between 0.1 and 0.9 V. The $TCNI_{p2}$ and the TCD are independent of V_a (22) and (26) and are around 15.9% $\cdot K^{-1}$ and −0, 01% $\cdot K^{-1}$. Then, the $TCLW_p$ (32) depends on V_a and is around 0.07% $\cdot K^{-1}$. Afterward, we consider that TCD and $TCLW_p$ can be neglected compared to TCC_{diff}. Indeed, in most cases, the sum of these terms is lower than 5% of TCC_{diff}. This affirmation is valid when W_p is smaller than l_p such as $W_p < 0.95\ l_p$. In this case, we modify equation (18) for the TCC_{diff} of n^+p diode

$$TCC_{diff} = TCNI_{p2} - \frac{qV_a}{kT^2}. \quad (33)$$

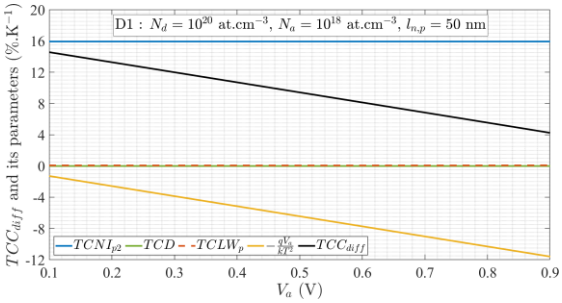

Fig. 1. Evolution of the temperature coefficient of diffusion current and its parameters with the applied voltage for D1 at 300 K.

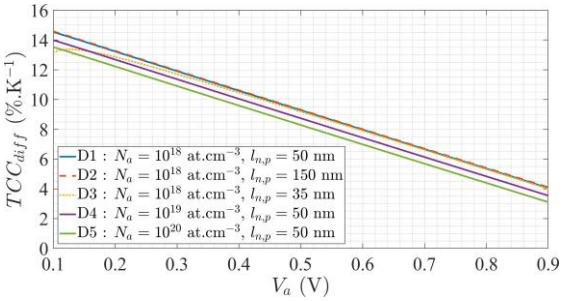

Fig. 2. Evolution of the temperature coefficient of diffusion current as a function of the applied voltage for D1, D2, D3, D4, and D5 at 300 K.

The formulation obtained in (33) is similar to the TCC_{diff} of long diodes found in the literature [9], [13].

Finally, the influences of $N_{a,d}$ and $l_{p,n}$ are represented (Fig. 2). This Figure shows the TCC_{diff} (17) for five diodes as a function of V_a at 300 K where $N_d = 10^{20}$ at $\cdot$ cm^{-3}.

In Fig. 2, $N_{a,d}$ and $l_{p,n}$ have a significant influence on the TCC_{diff}. For the same V_a, the TCC_{diff} is higher when N_a is smaller. There is a rise of 1% $\cdot$ K^{-1} when N_a decreases from 10^{20} to 10^{18} at $\cdot$ cm^{-3}. Concerning $l_{p,n}$, the TCC_{diff} diminishes when $l_{p,n}$ decreases from 150 to 35 nm. This change is only seen when V_a is lower than 0.4 V and can be correlated to cases where (33) is not valid.

B. Temperature Coefficient of Recombination Current

In the case of $J = J_{rec}$, the TCC is expressed as follows:

$$TCC_{rec} = \frac{1}{J_{rec}} \frac{dJ_{rec}}{dT}. \quad (34)$$

Then, using (10) and (11), (34) is discriminated into different physical parameters such as TCC_{diff}

$$TCC_{rec} = 1 + TCNI - TCF_{np} - TC\tau - \frac{qV_a}{2kT^2} \quad (35)$$

where TCNI, TCF_{np} and $TC\tau$ are the temperature coefficients of n_i, F_{np} and τ.

If p^+n or n^+p diodes are considered, $J_{rec-sat}$ depends only on P or N region. For a n^+p diode, (35) is approximated

$$TCC_{rec} = 1 + TCNI_p - TCF_{np} - TC\tau_p - \frac{qV_a}{2kT^2} \quad (36)$$

where $TCNI_p$ and $TC\tau_p$ are the temperature coefficients of n_{ip} and τ_p.

1) Temperature Coefficient of Concentration of Intrinsic Carriers: The $TCNI_{n,p}$ is simply obtained by using (26)

$$TCNI_{n,p} = \frac{1}{n_{in,p}} \frac{dn_{in,p}}{dT} = \frac{TCNI_{n2,p2}}{2}. \quad (37)$$

2) Temperature Coefficient of Electric Field: F_{np} is different for diodes with symmetrical ($N_a = N_d$) or asymmetrical ($N_a \neq N_d$) doping levels [18]. For a n^+p diode, F_{np} is equal to

$$F_{np} = \frac{qN_a(2V_{bip} - V_a)}{\epsilon_0\epsilon_r}^{1/2} \quad (38)$$

where V_{bip} is the built-in potential (V) in the space charge region W_p [18]. The TCF_{np} is obtained using (1) and (38)

$$TCF_{np} = \frac{1}{F_{n,p}} \frac{dF_{n,p}}{dT} = \frac{1}{2V_{bip} - V_a} \frac{dV_{bip}}{dT}. \quad (39)$$

For diodes with symmetrical doping levels, $2V_{bip}$ is equivalent to Φ_0 [18]. Therefore, TCF_{np} is equal to

$$TCF_{np} = \frac{1}{F_{n,p}} \frac{dF_{n,p}}{dT} = \frac{1}{2(\Phi_0 - V_a)} \frac{d\Phi_0}{dT}. \quad (40)$$

3) Temperature Coefficient of Minority Carrier Lifetimes: $\tau_{n,p}$ are calculated using the expressions of Law et al. [19]. Here, we choose to neglect the band-to-band Auger impact on the minority carrier lifetimes. Thus, the minority carrier lifetimes are only influenced by SRH mechanisms. Then, we assume that $\tau_{n,p}$ is proportional to T^η where $0 \leq \eta \leq 1.77$ between 300 and 400 K [20]. This expression is obtained

$$\tau_{n,p} = \frac{\tau_{300\,K}}{1 + \frac{N_T}{N_{ref}}} \left(\frac{T}{300}\right)^\eta \quad (41)$$

where $\tau_{300\,K}$ is the low concentration lifetime of charges carriers at 300 K (s), $N_{ref} = 10^{17}$ is the roll-off concentration (at $\cdot$ cm^{-3}), $N_T = N_{d,a}$ for N and P regions. Here, we choose to approximate η and fix its value to 1. Therefore, $TC\tau_n$ and $TC\tau_p$ are equal

$$TC\tau_{n,p} = \frac{1}{\tau_{n,p}} \frac{d\tau_{n,p}}{dT} = \frac{1}{T}. \quad (42)$$

4) Analysis of the Contributions to the Temperature Coefficient of Recombination Current: Fig. 3 illustrates the results of the TCC_{rec} of a n^+p diode at 300 K. This one is similar to the diode D1. Here, the low concentration lifetime of charge carriers at 300 K, $\tau_{300\,K}$ is equal to 10^{-8} s. The TCC_{rec} and its contributions (36) are represented as a function of V_a. In Fig. 3, the TCC_{rec} decreases from 7.7% $\cdot$ K^{-1} to 3.4% $\cdot$ K^{-1} when V_a is ranging from 0.1 to 0.85 V. For higher voltages the TCC_{rec} increases from 3.4% $\cdot$ K^{-1} to 4% $\cdot$ K^{-1}. The $TCNI_p$ and the $TC\tau_0$ are independent of V_a (37) and are about 8% $\cdot$ K^{-1} and 0.33% $\cdot$ K^{-1} respectively. Meanwhile, the TCF_{np} (39) depends on V_a and raises from 0.73% $\cdot$ K^{-1} to 2.05% $\cdot$ K^{-1}.

Finally, the influence of N_a is represented in Fig. 4. It shows the TCC_{rec} of three diodes at 300 K where $l = 50$ nm, $N_d = 10^{20}$ at $\cdot$ cm^{-3} and $\tau_{300\,K} = 10^{-8}$ s. As shown earlier in the diffusion regime, the TCC_{rec} evolves also with the doping level (Fig. 4). When N_a decreases from 10^{20} to 10^{18} at $\cdot$ cm^{-3},

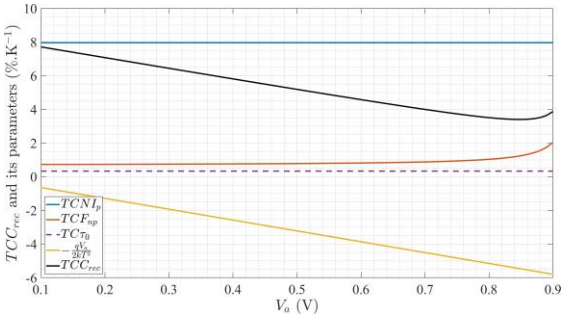

Fig. 3. Evolution of the temperature coefficient of recombination current and its parameters as a function of the applied voltage for D1 at 300 K.

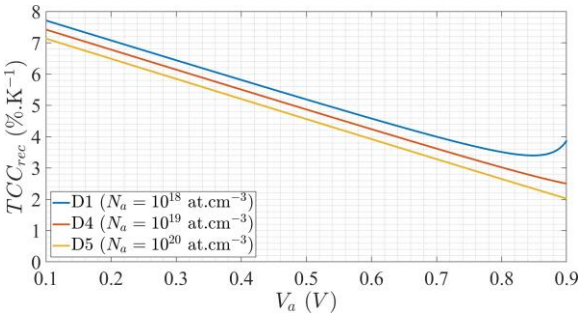

Fig. 4. Evolution of the temperature coefficient of recombination current as a function of the applied voltage for D1, D4, and D5 at 300 K.

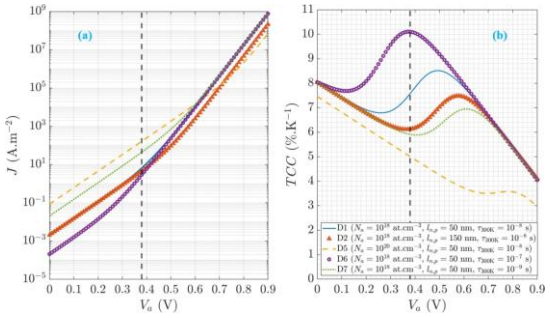

Fig. 5. (a) J-V characteristics and (b) TCC for D1, D2, D5, D6, and D7 at 300 K.

the TCC_{rec} increases of 0.6% · K^{-1}. Moreover, we note that the rise of the TCC_{rec} at high voltages is only present for D1. We attribute this to the TCF_{np} (39).

C. TCC in p-n Diodes

The expressions of TCC in different regimes of a p-n diode provide a complete form for the TCC. This form, independent of the studied regime, is obtained by using (2)

$$\mathrm{TCC} = \frac{J_{\mathrm{diff}}}{J} \times \mathrm{TCC}_{\mathrm{diff}} + \frac{J_{\mathrm{rec}}}{J} \times \mathrm{TCC}_{\mathrm{rec}}. \quad (43)$$

Fig. 5 presents the J–V characteristics and the TCC of five diodes at 300 K where $N_d = 10^{20}$ at cm^{-3}. The other parameters are displayed in the legend. In Fig. 5, the TCC always evolves in the same way with V_a. In the low injection regime, when $J = J_{\mathrm{rec}}$, the TCC decreases when V_a increases. Subsequently, when J_{diff} becomes close to J_{rec}, there is an elevation of the TCC when V_a increases. Finally, when $J = J_{\mathrm{diff}}$, the TCC decreases again as V_a increases. We also

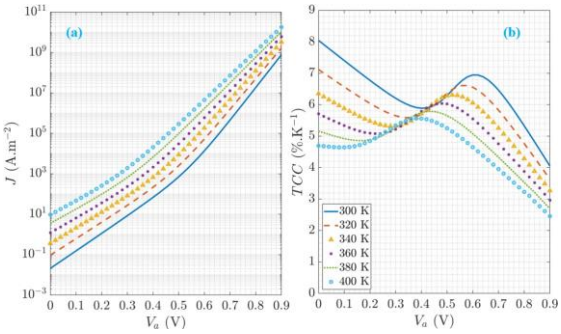

Fig. 6. (a) J-V characteristics and (b) TCC of D7 at 300-400 K.

define $V_{a-\mathrm{int}}$ which is the value of V_a where $J_{\mathrm{rec}} = J_{\mathrm{diff}}$. For D1, it is represented by a dashed black line in Fig. 5. $V_{a-\mathrm{int}}$ illustrates the transition between the TCC_{rec} and the TCC_{diff}. For instance, $V_{a-\mathrm{int}} = 0.38$ V for D1. The evolution of the TCC with the doping is consistent with the observations made earlier for the diffusion and recombination regimes. The doping also influences $V_{a-\mathrm{int}}$. In this case, $V_{a-\mathrm{int}}$ increases from 0.38 to 0.74 V when the doping increases from 10^{18} to 10^{20} at · cm^{-3}. The other parameters as $\tau_{300\ \mathrm{K}}$ and $l_{n,p}$ only change the value of $V_{a-\mathrm{int}}$. When the $l_{n,p}$ varies from 50 to 150 nm, $V_{a-\mathrm{int}}$ increases from 0.38 to 0.48 V. On the other hand, when $\tau_{300\ \mathrm{K}}$ raises from 10^{-9} to 10^{-7} s, $V_{a-\mathrm{int}}$ diminishes from 0.52 to 0.26 V. This last observation is due to the decrease of J_{rec} when $\tau_{300\,\mathrm{K}}$ increases (11).

Finally, Fig. 6 represents the J–V characteristics and the TCC of D7 ($N_d = 10^{20}$ at · cm^{-3}, $N_a = 10^{18}$ at · cm^{-3}, $l_{n,p} =$ 50 nm, $\tau_{300\,\mathrm{K}} = 10^{-9}$ s) at 300–400 K.

In Fig. 6, the TCC decreases as T increases. The reduction depends on V_a. For instance, the TCC reduces from 5.9% · K^{-1} to 5.6% · K^{-1} at 0.4 V and from 6.9% · K^{-1} to 4.5% · K^{-1} at 0.62 V. Moreover, we observe that $V_{a-\mathrm{int}}$ also decreases as T increases. Therefore, at high temperatures, the regime where the TCC_{rec} is dominant does not appear at low voltages.

III. Results and Discussion

To validate the analytical model (AM) of the TCC of a p-n diode, our results are compared to those obtained with Silvaco 2-D TCAD simulations. To design the different diodes, TCAD simulations are carried out on Victory Device using BGN, MASETTTI, and CONSRH models [27]. To correspond to (41), some parameters of CONSRH are fixed: TAUP = TAUN = 10^{-8} s, NSHRN = NSRHP = 10^{17} at · cm^{-3} and LT.TAUP = LT.TAUN = 1. Other used parameters are the default parameters of the models BGN, CONSRH, and MASSETTI [27]. We study two diodes: D1 where $N_a = 10^{18}$ at · cm^{-3}, $N_d = 10^{20}$ at · cm^{-3}, $l_{n,p} = 50$ nm, $\tau_{300\ \mathrm{K}} = 10^{-8}$ s and D5 where $N_{a,d} = 10^{20}$ at · cm^{-3}, $l_{n,p} = 50$ nm, and $\tau_{300\ \mathrm{K}} = 10^{-8}$ s. Fig. 7 presents a comparison between the J–V characteristics and the TCC of D1 and D8 obtained with the TCAD and our model at 300–400 K. In Fig. 7, there is a strong agreement between the model and TCAD simulations in the diffusion regime and the recombination regime. A discrepancy only appears in the transition between the two regimes. For D1, the maximal difference is about

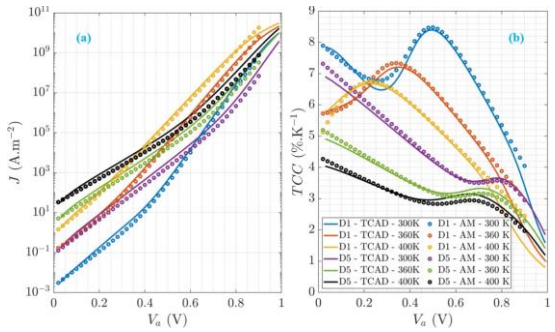

Fig. 7. (a) *J-V* characteristics and (b) TCC obtained with the AM and TCAD simulations for D1 and D5 at 300-400 K.

TABLE I
PHYSICAL PARAMETERS OF THE DIODES

Diode	Average doping (at.cm^{-3})	Silicon doping process	Length (μm)
Our work [28]	$N_a = 9 \times 10^{18}$ $N_d = 6 \times 10^{19}$	Epitaxy	$l_p = 0.08$ $l_n = 0.05$
Fournol et al [10]	$N_a = 4.6 \times 10^{19}$ $N_d = 1 \times 10^{17}$	Ion implantation	$l_p = 5$ $l_n = 1$

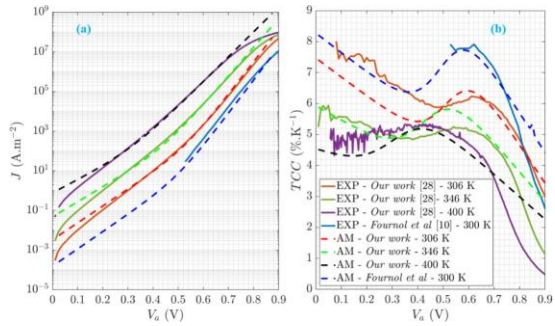

Fig. 8. (a) *J-V* characteristics and (b) TCC obtained with experimental results (EXP) and our AM at 300-400 K.

0.35%$\cdot$ K^{-1} at 0.3 V and 300 K. This dispersion of the TCC in the transition regime is due to the approximations of J_{rec} made in (9)–(11). In our model, U is uniform in W and is fixed thanks to F_{np} [18]. The TCAD does not use these approximations to express U.

Finally, we compare our AM to experimental results. In this article, the experimental results are derived from two diodes (Table I). The first set of results is derived from our work in [28] using Keysight B1500 A Semiconductor Device Parameter Analyzer and a Semiautomated four-probe system Cascade Microtech SUMMIT 12 000 at 300–400 K. The second one is taken from Fournol et al. [10] at 300 K. The J –V characteristics and the TCC of these two diodes are compared to our model as a function of V_a at 300–400 K (Fig. 8). In Fig. 8, we use the same lengths and average dopings as in Table I. The $\tau_{300\,\text{K}}$ is the only parameter used to fit the model with the experimental results. The $\tau_{300\ \text{K}}$ is about 5 4 10^{-9} s for our diode [28] and $4 \cdot 10^{-8}$ s for Fournol et al. [10]. There is a great agreement between the model and experimental results. For our diode, there is a strong correlation between the model and the experimental results at 306–400 K in the diffusion regime. Outside this regime, there is a discrepancy about 1%$\cdot$K^{-1} between the model and the experimental results at 300 K. We attribute this difference to two approximations made in our model. First, we use Boltzmann statistics instead of Fermi statistics for our equations. Second, we considered average doping in P and N regions instead of using the real doping profile in these regions. It shows the limit of our model when the doping is not constant in the P and N regions. At higher voltages, the experimental results are lower than the model. We attribute this difference to the influence of R_s which we neglected in our model. The disparity begins at 0.7 V at 400 K and 0.8 V at 346 K. In the case of Fournol et al. [10], there is a superposition of the two curves when V_a is between 0.5 and 0.8 V. Similar to our diode, there is a difference at high voltages due to R_s.

IV. CONCLUSION

This article presents an AM of the TCC in p-n short diodes between 300 and 400 K. We have demonstrated that the TCC is highly dependent on the conduction in the diode (recombination or diffusion). At a given voltage, the TCC of the recombination current is lower than the TCC of the diffusion current. For that reason, there is an increase of the TCC as the applied voltage grows only at the transition between the two conduction modes. When one of the two conductions becomes negligible, the TCC always decreases with the applied voltage. The TCC is written as a sum of several physical and technological contributions. This formalism is very useful to analyze the weight of each contribution to the TCC. It is also useful to estimate the voltage where the transition between the two conduction modes (diffusion and recombination) occurs. This transition depends strongly on the doping concentration and the length of the N and P regions. In both conduction modes, the intrinsic carrier concentration $n_{\text{ip},n}$ remains the main contribution to the TCC. Our AM has been finally compared and validated with TCAD simulations and experimental results. In general, for both diffusion and recombination currents, the matching between the model and the TCAD is excellent. However, discrepancies appeared at 300 K which can be explained by the approximations made in our model in the recombination current. Moreover, there is also a strong correlation between the model and the experimental results for different diodes. However, the model shows limits when the doping is not perfectly constant in the P and N regions. Finally, the deviation observed at high voltages is simply due to our approximations of the series resistance. These comparisons confirm the ability of the proposed model to accurately express the TCC of short silicon p-n diodes under low-level injections and at 300–400 K.

REFERENCES

[1] T. Huynh, "Fundamentals of thermal sensors," in *Thermal Sensors: Principles and Applications for Semiconductor Industries*, J. C. Mohan Ed., 1st ed. New York, NY, USA: Springer, 2015, ch. 2, sec. 2.1, pp. 5–42.

[2] P. W. Kruse and D. D. Skatrud, "Uncooled infrared imaging arrays and systems," in *Semiconductors and Metals*, vol. 47, R. K. Willardson and E. R. Weber Eds., 1st ed. San Diego, CA, USA: Academic Press, 1997.

[3] J. Love, *Process Automation Handbook: A Guide to Theory and Practice*, vol. 42, 1st ed. New York, NY, USA: Springer, 2015.

[4] C. Dames, "Resistance temperature detectors," in *Encyclopedia of Microfluidics and Nanofluidics*, L. Dongqing Ed., 1st ed. Boston, MA, USA: Springer, 2008, pp. 1782–1790.

[5] J. L. Tissot, "IR detection with uncooled sensors," *Infr. Phys. Technol.*, vol. 46, nos. 1–2, pp. 147–153, Dec. 2004, doi: 10.1016/j.infrared.2004.03.018.

[6] D. Fujisawa et al., "Development of new pixel structure for beyond 12-μm pixel pitch SOI diode uncooled IRFPAs," *Proc. SPIE*, vol. 11407, Apr. 2020, Art. no. 114071A, doi: 10.1117/12.2558287.

[7] A. Albouy, "Etude et évaluation de dispositifs FD-SOI sur structures suspendues pour des applications dans la bolométrie infrarouge," Ph.D. dissertation, Opt. Photon. Division, CEA Leti, Grenoble-Alpes Univ., Grenoble, FR, USA, 2022.

[8] S. Eminoglu, D. S. Tezcan, M. Y. Tanrikulu, and T. Akin, "Low-cost uncooled infrared detectors in CMOS process," *Sens. Actuators A, Phys.*, vol. 109, nos. 1–2, pp. 102–113, Dec. 2003, doi: 10.1016/j.sna.2003.08.013.

[9] J. Blond, "High performance terahertz detector for passive imaging," Ph.D. dissertation, Opt. Photon. Division, CEA Leti, Grenoble-Alpes Univ., Grenoble, FR, USA, 2021. [Online]. Available: https://www.theses.fr/2021GRALT062

[10] A. Fournol, J. Blond, A. Aliane, H. Kaya, J. Meilhan, and L. Dussopt, "Thermal sensing performances of thin-film lateral PiN diodes at 80 K and 300 K," in *Proc. IEEE 52nd Eur. Solid-State Device Res. Conf. (ESSDERC)*, Sep. 2022, pp. 285–288, doi: 10.1109/ESSDERC55479.2022.9947136.

[11] M. Mansoor, I. Haneef, S. Akhtar, A. De Luca, and F. Udrea, "Silicon diode temperature sensors—A review of applications," *Sens. Actuators A, Phys.*, vol. 232, pp. 63–74, Aug. 2015, doi: 10.1016/j.sna.2015.04.022.

[12] J.-K. Kim and C.-H. Han, "A new uncooled thermal infrared detector using silicon diode," *Sens. Actuators A, Phys.*, vol. 89, nos. 1–2, pp. 22–27, Mar. 2001, doi: 10.1016/s0924-4247(00)00532-x.

[13] E. Fuxa, "Etude théorique du dimensionnement d'une matrice bolométrique Au pas de 5 μm, par report de dispositifs SOI sur structures suspendues pour des applications dans l'imagerie infrarouge non refroidi," Ph.D. dissertation, Opt. Photon. Division, CEA Leti, Grenoble-Alpes Univ., Grenoble, FR, USA, 2016.

[14] J. P. Colinge and C. A. Colinge, *Physics of Semiconductor Devices*, 1st ed., New York, NY, USA: Springer, 2002, ch. 1, pp. 1–137, doi: 10.1007/b117561.

[15] S. M. Sze and K. Ng. Kwok, *Physics of Semiconductor Devices*, 3rd ed. Hoboken, NJ, USA: Wiley, 2006, pp. 1–196, doi: 10.1002/0470068329.

[16] W. Shockley and W. T. Read, "Statistics of the recombinations of holes and electrons," *Phys. Rev.*, vol. 87, pp. 835–842, Sep. 1952.

[17] C.-T. Sah, R. Noyce, and W. Shockley, "Carrier generation and recombination in P-N junctions and P-N junction characteristics," *Proc. IRE*, vol. 45, no. 9, pp. 1228–1243, Sep. 1957, doi: 10.1109/JRPROC.1957.278528.

[18] M. Shur, "Recombination current in forward-biased p-n junctions," *IEEE Trans. Electron Devices*, vol. 35, no. 9, pp. 1564–1565, Sep. 1988, doi: 10.1109/16.2595.

[19] M. E. Law, E. Solley, M. Liang, and D. E. Burk, "Self-consistent model of minority-carrier lifetime, diffusion length, and mobility," *IEEE Electron Device Lett.*, vol. 12, no. 8, pp. 401–403, Aug. 1991, doi: 10.1109/55.119145.

[20] D. B. M. Klaassen, "A unified mobility model for device simulation—II. Temperature dependence of carrier mobility and lifetime," *Solid-State Electron.*, vol. 35, no. 7, pp. 961–967, Jul. 1992, doi: 10.1016/0038-1101(92)90326-8.

[21] F. J. Morin and J. P. Maita, "Electrical properties of silicon containing arsenic and boron," *Phys. Rev.*, vol. 96, no. 1, pp. 28–35, Oct. 1954, doi: 10.1103/physrev.96.28.

[22] G. W. Ludwig and R. L. Watters, "Drift and conductivity mobility in silicon," *Phys. Rev.*, vol. 101, no. 6, pp. 1699–1701, Mar. 1956, doi: 10.1103/physrev.101.1699.

[23] G. Masetti, M. Severi, and S. Solmi, "Modeling of carrier mobility against carrier concentration in arsenic-, phosphorus-, and boron-doped silicon," *IEEE Trans. Electron Devices*, vol. ED-30, no. 7, pp. 764–769, Jul. 1983, doi: 10.1109/T-ED.1983.21207.

[24] Y. P. Varshni, "Temperature dependence of the energy gap in semiconductors," *Physica*, vol. 34, no. 1, pp. 149–154, Jan. 1967, doi: 10.1016/0031-8914.

[25] N. A. Gokcen, "Statistical thermodynamics of electrons and holes in semiconductors," *J. Chem. Phys.*, vol. 83, no. 3, pp. 1240–1245, Aug. 1985, doi: 10.1063/1.449439.

[26] J. W. Slotboom, "The pn-product in silicon," *Solid State Electron.*, vol. 20, no. 4, Apr. 1977, pp. 279–283, doi: 10.1016/0038-1101(77)90108-3.

[27] *Victory Device—User Manuel*, Santa Clara, CA, USA: Silvaco, 2021, ch. 3, pp. 51–328.

[28] R. M. R. Kubica et al., "Epitaxial p^+n^+ vertical short diodes for microbolometers," in *Proc. 10th EuroSOI-ULIS Conf.*, May 2024.